UNIVERSITY OF CALIFORNIA

SANTA CRUZ

ADVANCED MATERIALS AND NANO TECHNOLOGY FOR SOLAR CELLS

A thesis submitted in partial satisfaction
of the requirements for the degree of

MASTER OF SCIENCE

in

Electrical Engineering

by

Tao Han

June 2014

The Thesis of Tao Han
is approved:

_____
Professor Michael M. Oye, Chair

_____
Professor Michael Isaacson

_____
Professor Holger Schmidt

_____
Tyrus Miller
Vice Provost and Dean of Graduate Studies

TABLE OF CONTENTS

Table of Figures

ABSTRACT

TAO HAN

ADVANCED MATERIALS AND NANO TECHNOLOGY FOR SOLAR CELLS

In order to optimize the optical and electronic properties of solar cells and enhance the conversion efficiency, this article mainly investigated the advanced optoelectronic materials which play important role in photovoltaic devices. The physical mechanism and their potential applications are systematically studied. The optical and electronic properties are tuned and optimized by co-doping some elements or adding silver nanoparticles into the semiconductor films. The research methods involve chemical deposition growth of the materials, measurements and analysis of the properties, modeling and simulation based on electrodynamics, quantum mechanics with many body theory, semiconductor physics and optics, and finally the comparison from these different research methods. On one hand, experimentally and theoretically, the semiconductor co-doped with IIA and IIIA elements was found to be widely tunable for its band gap and resistivity, and thus has great potential in the field of photovoltaics and microelectronics. On the other hand, theoretically, it was shown that the optical properties of semiconductors with silver nanoparticles rely on the particle scale and distribution density, providing the theoretical guidance for the Ag nano based multifunctional materials.

DEDICATION AND ACKNOWLEDGEMENT

I take this opportunity to express thanks to those who made a difference in my life during the two years at UCSC. First and foremost, I would like to thank Dr. Michael M. Oye for my research and thesis. He provided me the complete support from the choice of the research topic and till its completion. He kept providing me the timely motivation and proper guidance to pursue the thesis. I also would like to thank my reading committee members Dr. Michael Isaacson and Dr. Holger Schmidt for spending their valuable time reading my thesis and providing feedback. Last but not the least, I would thank my parents and friends for their constant support for my research and thesis.

1. INTRODUCTION

1.1 SIGNIFICANCE OF PHOTOVOTAICS

1.1.1 WORLDWIDE ENERGY PROBLEMS

Modern material civilization emerged from the industrial revolution with unparalleled prosperity in the last two decades. The global modernization has been always relied on the fossil energy sources such as oil, coal, natural gas and nuclear fission. At our current rate of consumption, the remaining reserves and durable years of the main conventional energy are listed in Table 1-1[1].

Table 1-1. World energy reserves and durable years

Type	Estimated reserves	Annual consumption	Durable years
Oil	2.2×10^{11} tons	3.2×10^{9} tons	69 years
Coal	9.5×10^{11} tons	1.5×10^{10} tons	63 years
Natural gas	$1.9\times10^{14}\,m^3$	$2.3\times10^{12}\,m^3$	82 years

The annual production capacity of uranium is about 60, 000 tons, which can last until 2030 according to the estimation of World Energy Council.

Fossil energy results in many environmental problems. Thousands of tons of hazardous substances are released to the air every year from the combustion of coal and petroleum. The acid rain emerges in some areas severely pollutes the water and soil. The utility of

fossil energy also produces greenhouse gases and results in global warming. Figure 1-1 shows the map of global warming[2].

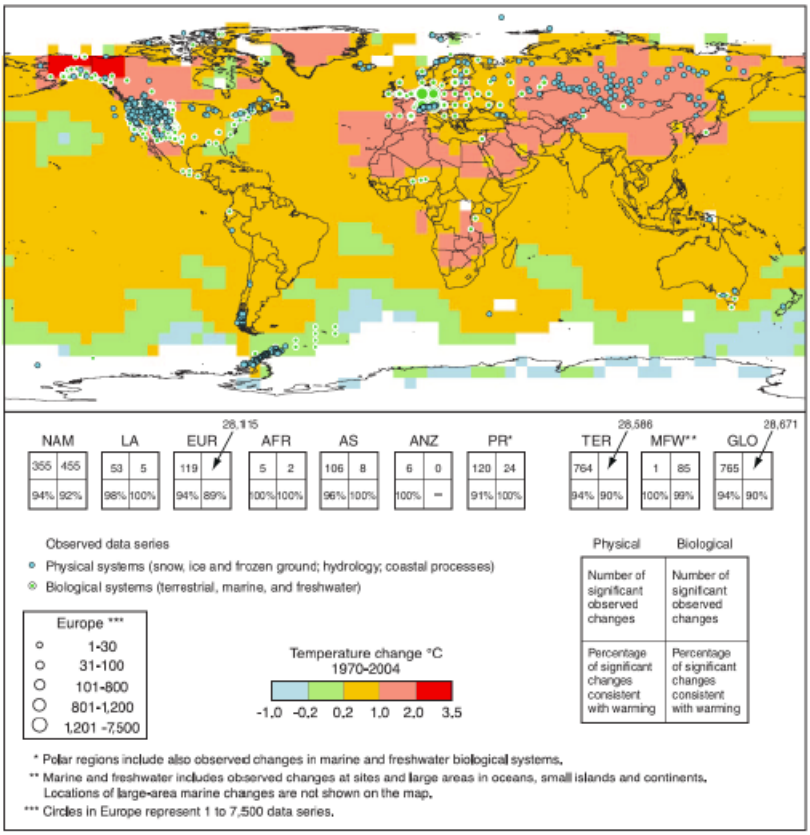

Figure 1-1. Changes in physics and biology system and surface temperature 1970-2004

Thus, human beings are facing the pressure of economic development, environmental protection, and energy conservation. There is no doubt that discovering sustainable renewable energy has become a worldwide need.

1.1.2 SOLAR ENERGY AND SOLAR CELLS

Essentially, all of the creatures on the earth are fed by the solar energy with almost all the sources of energy being bio-energy, wind energy and hydro-energy that come from the solar energy. The power released by the sun is about 1.6×10^{23}kw. The part that the earth receives per second is as high as 8×10^{13}kw, is the equivalent of 6×10^{9} tons of standard coal. By this measure, the annual solar energy received by the earth is the equivalent of 1.9×10^{17} tons of standard coal, which is beyond 10,000 times of the coal reserves. The sun supplies the energy continually to the earth, and the solar energy is a sort of inexhaustible resource.

In addition, the solar energy has many advantages. First, many countries which are short of conventional energy have abundant solar energy. Second, solar energy is a clean energy. Its development and utilization almost never brings pollution problems. Therefore, solar energy is a very promising resource to replace conventional energy. More and more experts in the area of power and energy predict that solar energy will be the mainstream in the future 50 years. The prediction of the future energy supply is shown in Figure 1-2[3].

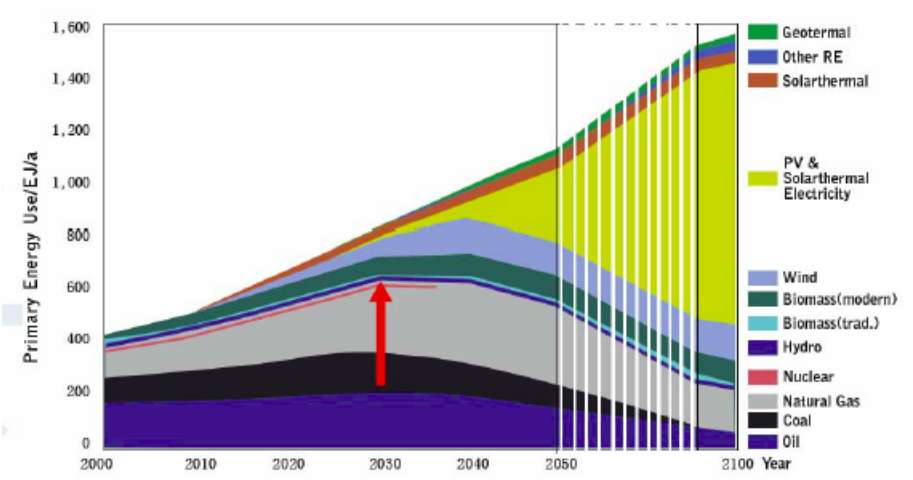

Figure 1-2 Energy supply prediction by European Commission's Joint Research Center

1.2 AN OVERVIEW OF SOLAR CELLS

1.2.1 HISTORY OF SOLAR CELLS

The first solar cell was discovered by the French physicist, Edmond Becquerel in 1839. He found that the voltaic cell made of two pieces of metal immersed in the solution will gain addition electrodynamic potential when the cell was illuminated by the sun. This is called Photovoltaic Effect. In 1883, Fritts brought up the first solar cell made by selenium. In 1954, the first practical solar cell was invented by Bell Labs and the cell was made by silicon with a p-n junction structure. The efficiency was soon improved to 10%, creating a new era in solar cell development. In 1958, solar cells were first applied to the satellite.

Over the last fifteen years, the production capacity of solar cells have increased by nearly ten times, and the price has been reduced by 3/4.

1.2.2 SOLAR CELL CLASSIFICATION

Generally, solar cells achieve the Photovoltaic Effect using a specific potential barrier and convert the solar energy into the electric power. Solar cells are usually sorted by the structure and materials.

(1) Sorted by structures

a. Homo-junction solar cells: made up of one type of semiconductor material, consist one or more p-n junction. Example: Si solar cell, GaAs solar cell.

b. Heterojunction solar cells: made up of over two kinds of semiconductor materials. Example: Cu_2S/ CdS solar cell.

c. Schottky junction solar cell: with a metal/ semiconductor interface forming the Schottky junction. Example: metal oxide semiconductor solar cell.

d. Photoelectric chemistry cell: made up of semiconductor electrodes immersing in solution.

(2) Sorted by materials

a. Crystalline-Si solar cell: crystalline silicon cell is the dominating type of solar cell in photovoltaic industry since its high efficiency, stability, and long life. The silicon solar cells with the efficiency of 24.7% prepared in the lab still keep the efficiency record

except for GaAs solar cells[4]. The c-Si solar cells of industry usually have a efficiency of 13-16%.

b. Polycrystalline-Si solar cell: usually made up of polycrystalline Si wafer with the thickness of 350-450 μm. The wafer is cut from the ingot and waste lots of raw materials. In order to avoid the waste, researchers invented the p-Si thin film solar cell with the preparing method such as Low Pressure Chemical Vapor Deposition(LPCVD) or Plasma Enhanced Chemical Vapor Deposition (PECVD). The efficiency of p-Si solar cells of industry have been reached as high as 11-15%[5].

c. Amorphous-Si thin film solar cell: the amorphous silicon thin films have the advantage of low cost and easy to prepare in large scale. The thickness of a-Si thin films is usually 1 μm, which is only 1/300 of c-Si solar cells. This greatly reduced the material cost. The preparing process needs a low temperature of about 200oC. The energy consumption is very low. But the a-Si thin film solar cell has the shortcoming of insensitivity of long wavelength due to its wide band gap (1.7eV).

d. a-Si/ c-Si heterojunction(HIT) solar cells: another way to reduce the cost is to investigate a-Si/ c-Si heterojunction solar cells. The HIT solar cell is composed of a mono thin crystalline silicon wafer surrounded by ultra-thin amorphous silicon layers. The technology to add the intrinsic layer changed the performance of p-n junctions. HIT solar cells have the advantage of low temperature process, high efficiency, high stability

and low cost. Sanyo claimed that their HIT solar cells have achieved the efficiency of 21.4%. Figure 1-3 shows the comparison of traditional c-Si solar cell and HIT solar cell[6].

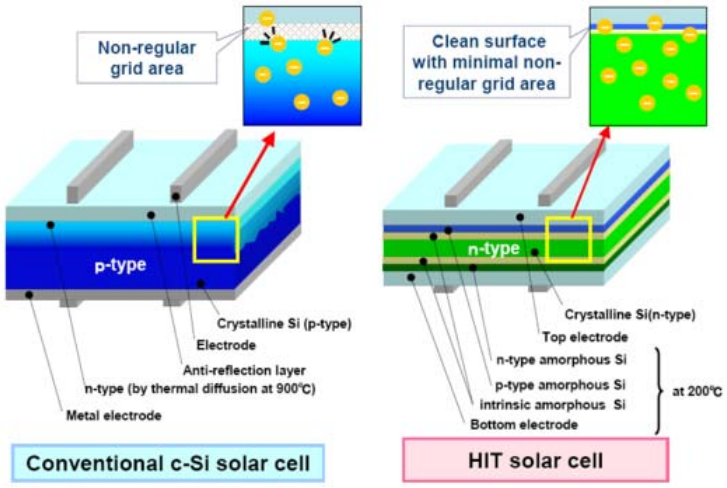

Figure 1-3. The structure diagram of c-Si solar cell and HIT solar cell

e. Copper indium selenide (CIS), Copper indium gallium selenide (CIGS) thin film solar cell: In 1977, the University of Maine prepared the first CIS thin film solar cell. Though over thirty years have been past, the CIS solar cell still does not serve useful purpose for the industry from due to production difficulties. Recently, Tokyo Institute of Technology prepared a novel CIGS solar cell using InSe to replace CdS and achieve the efficiency of 13.0%. But In Se, and Ga are relatively rare elements in the earth's crust, compared to other common solar cell elements such as silicon. There is still a long way to go for CIS, CIGS solar cells[7].

f. CdTe thin film solar cell: CdTe is a type of II-VI compound semiconductor materials. It is an ideal material for photoelectric conversion. The band gap of 1.45eV leads to a

very high absorption coefficient. The thin films with the thickness of 1 μm can absorb 99% photons from the incident sunlight. In 2001, the National Renewable Energy Laboratory prepared the solar cells with the efficiency of 16.4%, which keeps the highest record of CdTe thin film solar cells. But the development of CdTe thin film solar cell is still unsatisfied due to stability problems and difficulty with preparation[8].

2. PRINCIPLES OF SOLAR CELLS

2.1 PHOTOELECTRIC CONVERSION

Basically, there are three physical processes for photoelectric conversion in solar cells. First, the reflection and refraction of photons happen at the interface of the air and the semiconductor. Second, the photons stimulated the electron-hole pairs. Third, the non-equilibrium carriers are separated by the built in potential field.

When a beam of monochrome light shines on the surface of the semiconductor, a fraction of the intensity is reflected and the remaining fraction goes into the semiconductor. The semiconductor is able to absorb light and the refractive index $N = n - ik$ is wavelength dependent. For vertical incidence to the surface of semiconductor, the reflection has the relation with n and k as $r=[(n-1)^2+k^2]/[(n+1)^2+k^2]$ from Fresnel's Law[9]. For the interface between the air and the intrinsic silicon, the reflection is over 30%.

When the photons are absorbed by the semiconductor, the electrons at the valance band gain the photon energy and jump to the conduction band. At the same time a hole appears at the valance band. This process is called intrinsic absorption. The condition for intrinsic

absorption is that the photon energy must be larger than the band gap of the semiconductor. Therefore, each of semiconductor has its own absorption limit: $\lambda_0 = \mathrm{hc} / E_g$. The photons with a wavelength greater than λ_0 cannot be absorbed. λ_0 is about 1100nm for intrinsic c-Si, and 700nm for intrinsic a-Si. The absorption coefficient has the following relation: $\alpha = 4\pi\mathrm{k} / \lambda$.

2.2 PHOTOVOLTAIC EFFECT AND SILICON SOLAR CELLS

The principle diagram of silicon solar cells is shown in Figure 2-1. With light of proper wavelength shinning on the semiconductor devices, the photon energy is absorbed and the electrodynamic potential is generated. This phenomenon is called the Photovoltaic Effect. And solar cells are also called photovoltaic cells.

Each silicon atom has four outer electrons. With enough external energy, the outer electron can escape from the atom and becomes a free electron. And a hole appears in the atom. Doping elements such as B or Ga have the ability to capture electrons and the semiconductor become p-type (holes). Inversely, doped with the elements such as P or As, the semiconductor turns to be n-type (electrons).

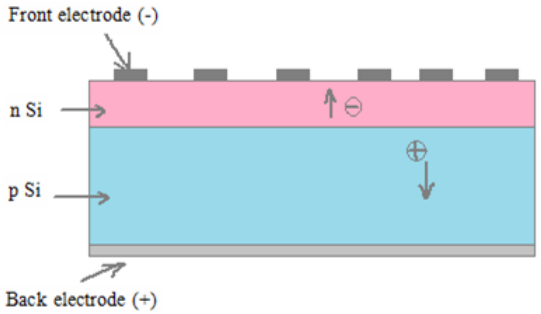

Figure 2-1 Diagram of silicon solar cells

If a piece of p-type silicon is placed in intimate contact with a piece of n-type silicon, then a diffusion of electrons occurs from the region of high electron concentration (the n-type side of the junction) into the region of low electron concentration (p-type side of the junction). When the electrons diffuse across the p-n junction, they recombine with holes on the p-type side. The diffusion of carriers does not happen indefinitely, however, because charges build up on either side of the junction and create an electric field. The electric field creates a diode that promotes charge flow, known as drift current, that opposes and eventually balances out the diffusion of electrons and holes. This region where electrons and holes have diffused across the junction is called the depletion region because it no longer contains any mobile charge carriers. It is also known as the space charge region[10].

2.3 HIT SOLAR CELLS

2.3.1 THEORY OF HIT SOLAR CELLS

Figure 2-2 is the diagram of HIT solar cells. The pin junction consists of three differently doped regions. As the name suggests, there is an intrinsic or undoped layer sandwiched between a p and an n doped region. When all layers are in contact, the Fermi levels of the doped regions must align on the same height. This provides a built in potential in the pin junction. The photons with the energy over the band gap of a-Si are absorbed by the pin junction. The electron-hole pairs are generated in the photovoltaic charge region and separated by the built in potential. Finally, the photovoltaic potential is generated and the direction is opposite to the built in potential[11].

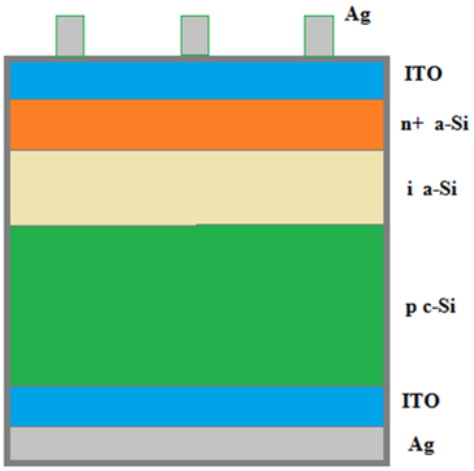

Figure 2-2 Structure of HIT solar cells

2.3.2 MAIN FACTORS AFFECTING THE EFFICIENCY

a. Optical loss: part of the incident light is reflected or transmitted.

b. Thermal conversion loss: For the photons with the energy larger than the band gap, $h\nu - E_g$ is positive and this part will generate phonons and deliver the energy to the lattice as heat.

c. Collection loss: Generally, the electron-hole pairs can be collected only if their distance from the space charge region is less than one diffusion length. And the electron-hole pairs that do not satisfy this condition will recombine, including the surface recombination and the bulk recombination.

d. Series resistance loss: The resistance comes from the bulk resistance, thin layer resistance, and electrode contact resistance. The series resistance not only consumes the

photovoltaic voltage, but also increases the temperature of the solar cell and decreases the output power[12].

3. BLACK SILICON TECHNIQUES

3.1 PHYSICAL PRINCIPLES

3.1.1 LOCALIZED SURFACE PLASMON

Surface plasmon resonance (SPR) is the coherent oscillation of free electrons of the materials stimulated by the incident photons. Metal with a small positive imaginary refractive index have this extraordinary property[13]. There is localized surface plasmon (LSP) when the size of the SPR material is smaller than the wavelength. Most of the electromagnetic energy is confined near the surface of the nanoparticles and the field intensity is greatly enhanced.

Over one hundred years ago, scientists discovered LSP from Ag and Au nanoparticles. The optical properties of the bulk metal materials should be very high reflectivity and short electromagnetic decay length. But the gold and silver nanoparticles exhibit a quit different characteristic: very high extinction of light.

LSP has now found interest in the fields of optics and material science, and it has been applied to multi disciplinary fields such as optical sensing and imaging devices.

3.1.2 OPTICAL PROPERTIES OF SILVER

Silver has long been valued as a precious metal, used in currency coins, to make jewelry, and as an investment in the forms of coins and bullion. Silver metal is used industrially in electrical contacts and conductors, in mirrors and in catalysis of chemical reactions. Its compounds are used in photographic film and dilute silver nitrate solutions and other silver compounds are used as disinfectants and microbiocides.

Silver in nanoscale is an ideal LSP material since its specific refractive index. The imaginary part is small. Figure 3-1 shows the experimental value of the refractive index of Ag[14]. Theoretically, this fundamental optical parameter can be calculated using Drude Model and there is a very good fit with the experimental value[15].

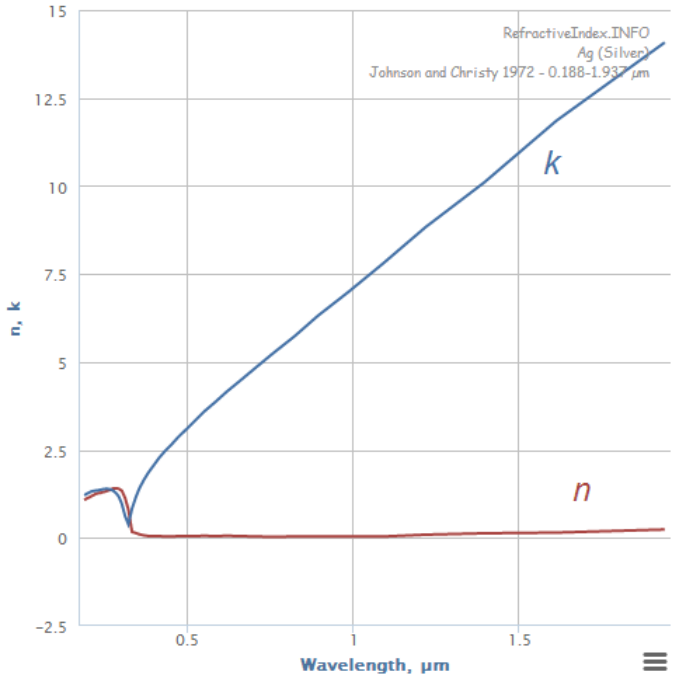

Figure 3-1 The refractive index of Ag

3.2 SILVER NANO PARTICLES

3.2.1 METHODOLOTY

a. For single Ag nanoparticle: In 1908, Gustav Mie obtained the rigorous analytic solution of the scattering of electromagnetic radiation by a sphere based on Maxwell Equations. Though deduced from the single particle, MIE theory is also applicable to randomly distributed particles when these spheres have the same radius and material composition because they do not have any phase correlations. MIE theory has a high practical value and it can be used for the scattering of metal nanoparticles, metal oxide nanoparticles, composite nanoparticles, atmosphere dust, colloidal suspension and so on[16].

For single spherical metal nanoparticle, the scattering solution can be obtained with MIE theory. Equations (1)-(5) show the expressions of scattering, absorption and extinction coefficient.

$$Q_{sca} = \frac{C_{sca}}{\pi R^2} = \frac{2}{x^2}\sum_{n=1}^{\infty}(2n+1)(|a_n|^2 + |b_n|^2), \quad (1)$$

$$Q_{ext} = \frac{C_{ext}}{\pi R^2} = \frac{2}{x^2}\sum_{n=1}^{\infty}(2n+1)\,\mathrm{Re}\{a_n + b_n\}, \quad (2)$$

$$Q_{abs} = Q_{ext} - Q_{sca}, \quad (3)$$

$$a_n = \frac{m^2 j_n(mx)[xj_n(x)]' - j_n(x)[mxj_n(mx)]'}{m^2 j_n(mx)[xh_n^{(1)}(x)]' - h_n^{(1)}(x)[mxj_n(mx)]}, \quad (4)$$

$$b_n = \frac{j_n(mx)[xj_n(x)]' - j_n(x)[mxj_n(mx)]'}{j_n(mx)[xh_n^{(1)}(x)]' - h_n^{(1)}(x)[mxj_n(mx)]}. \quad (5)$$

where λ is the wavelength, R is the radius, $x = \frac{2\pi R}{\lambda}$ is the shape factor, $j_n(x)$ is the Bessel function, $h_n^{(1)}$ is the Hankel function of the first kind, $m = M(\lambda) + iK(\lambda)$ is the refractive index of the particle, and $\mathrm{Re}\{a_n + b_n\}$ means the real part of $a_n + b_n$.

For the numerical solution of single Ag nanoparticle, the approximation of sphere is made. The study focuses the radius from 50 nm to 150 nm. Within this range, the structure is not necessary to consider and the refractive index can be used directly. Since the three coefficients can be expressed in series, it is very convenient to get the numerical solutions using Matlab.

b. For randomly distributed Ag nanoparticles in semiconductor thin films:

The Beer-Lambert Law states that there is a logarithmic dependence between the transmission (or transmissivity), T, of light through a substance and the product of the absorption coefficient of the substance, α, and the distance the light travels through the material (i.e., the path length), ℓ. The absorption coefficient can, in turn, be written as a product of either a molar absorptivity (extinction coefficient) of the absorber, ε, and the molar concentration c of absorbing species in the material, or an absorption cross section, σ, and the (number) density N' of absorbers. These relations are usually written as[17]:

$$\mathrm{T} = I / I_0 = e^{-\alpha l} = e^{-\sigma N l}. \qquad (6)$$

Applying the Beer-Lambert Law, the resulting transmittance intensity through a thin films embedded with randomly distributed particles is:

$$T = I / I_0 = e^{-C_{ext} Nl}, \quad (7)$$

where $C_{ext} = Q_{ext} \cdot \pi R^2$ is the extinction cross section, N is the particle density, and l is the thickness of the thin film[18]. Let f be the volume filling factor of the Ag nanoparticles in the thin films. Obviously $N = 3f / 4\pi R^3$. Then $T = e^{-\alpha l}$ where $\alpha = 3f \cdot Q_{ext} / 4R$ is the light absorption coefficient of the composite thin film.

3.2.2 RESULTS AND DISCUSSIONS

The extinction coefficient is calculated (Figure 3-2). All the minimum positions are at around 320nm where the extinction is weakest. With the increase of the radius, the dipole peak positions have an evident red shift. From the plasmonic theory, the red shift is reasonable because the oscillation electrons have a longer relaxation time for the particle with a larger radius. So the oscillation is lowered and the red shift appears.

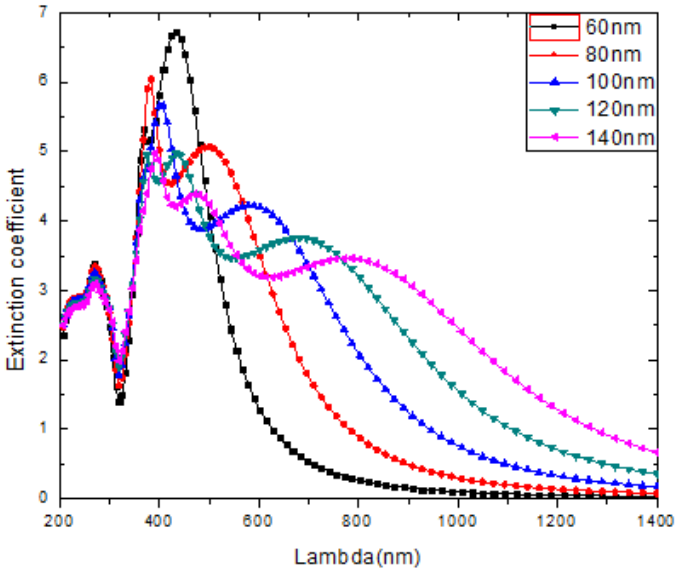

Figure 3-2. Extinction coefficient of single Ag nanoparticle with different radius

For solar cells, the light source is the sunshine. The solar cells utilize the standard AM1.5[19] spectrum usually from 300nm to 1100nm. The optimized extinction coefficient curves should be match with this spectrum and this can be easily realized by tuning the radius of the particle. The best Ag nanoparticle radius for silicon based solar cells is found to be about 100nm.

Figure 3-3 shows the extinction, absorption and scattering of the Ag nanoparticle with the radius of 100nm. It is clearly shown that almost all the extinction part comes from the scattering part and the absorption part is negligible. So the heat loss caused by the nanoparticle is very small and can be neglected.

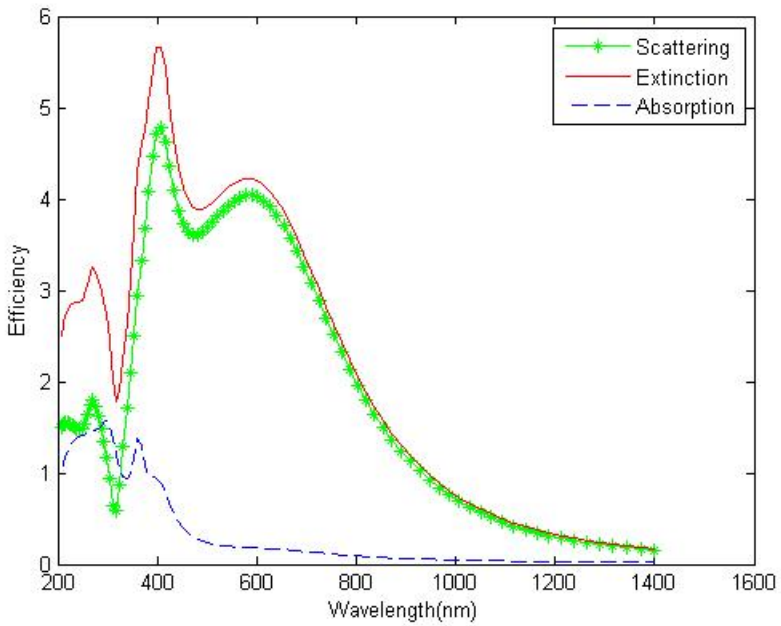

Figure 3-3. The coefficients of the 100nm radius Ag nanoparticle

The plasmonic layer consists of the intrinsic a-Si thin film with randomly distributed Ag nanoparticles. We set the volume filing factor f=0.1 and the radius R=100nm. The absorption coefficient is calculated. Figure 3-4 shows the absorption coefficient of the plasmonic layer compared with the intrinsic layer without nanoparticles. The absorption coefficient is significantly enhanced using the plasmonic structures in the visible wavelength. Thus, this design of the intrinsic layer has a great application potential for solar cells.

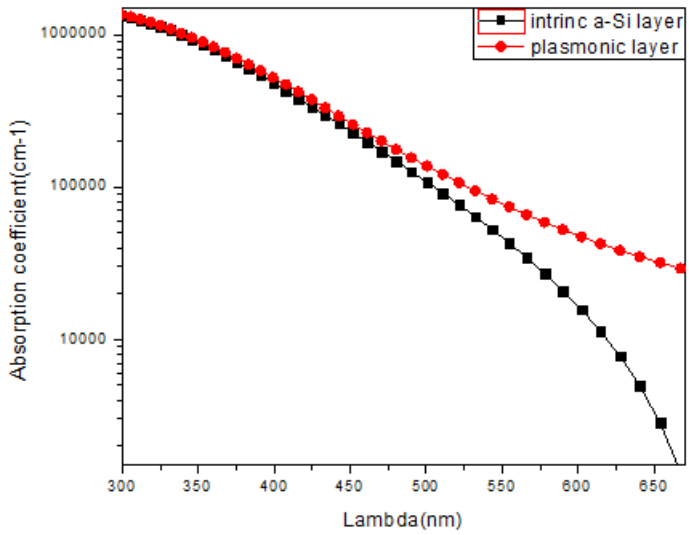

Figure 3-4 The absorption coefficient of the plasmonic layer and the intrinsic layer

3.3 APPLICATIONS IN SOLAR CELLS

3.3.1 MODELING METHODOLOGY

The boundary condition problems frequently appear in the physical system where electromagnetic field is involved. How to get the numerical solutions fast and effectively is a very important topic. One of the most powerful method to simulate the electromagnetic system and to solve the boundary condition problems is finite element method[20]. Most electromagnetic problems can be expressed as (8).

$$\mathrm{L}\Phi = g, \qquad (8)$$

where L is differential or integral operator, g is stimulant function, and Φ is field function we need to solve. Generally, boundary conditions include Dirichlet, Newman, and radiation boundary condition. Properties of time harmonic electromagnetic field can be expressed as (7) and (8), Helmholtz equation.

$$\nabla \times \left(\mu_{\mathrm{r}}^{-1} \nabla \times E(r)\right) - k_0^2 \varepsilon_r E(r) = -jk_0 Z_0 J, \qquad (9)$$

$$\nabla \times \left(\varepsilon_{\mathrm{r}}^{-1} \nabla \times H(r)\right) - k_0^2 \mu_r H(r) = \nabla \times \varepsilon_{\mathrm{r}}^{-1} J, \qquad (10)$$

Since there is no analytical solution for electromagnetic problems in practical engineering area, approximation methods have been developed. Galerkin method and Ritz method were the most frequently used approximation methods at the early stage solving electromagnetic field. And they are also the important methods to establish the finite element equations.

Generally, the finite element method include the following steps:

a. Establishing the differential equations and boundary conditions.

b. Building the discrete grids.

c. Choosing base functions and weighted functions. Converting the equations into linear equations by using Galerkin method or Ritz method.

d. Eliminating unknown quantities of the boundary and solving the matrix equations.

e. Post-processing and getting required parameters.

3.3.2 MONOCRYSTALLINE SILICON SOLAR CELLS WITH SILVER NANOPARTICLES

For monocrystalline Si solar cells, preparing light trapping structures onto the top surface is a simple and effective way to enhance the conversion efficiency because it improves the light current through the pn junction. In Fig. 3-5, silver nanoparticles are prepared onto the Si_3N_4 passivation layer of the solar cell.

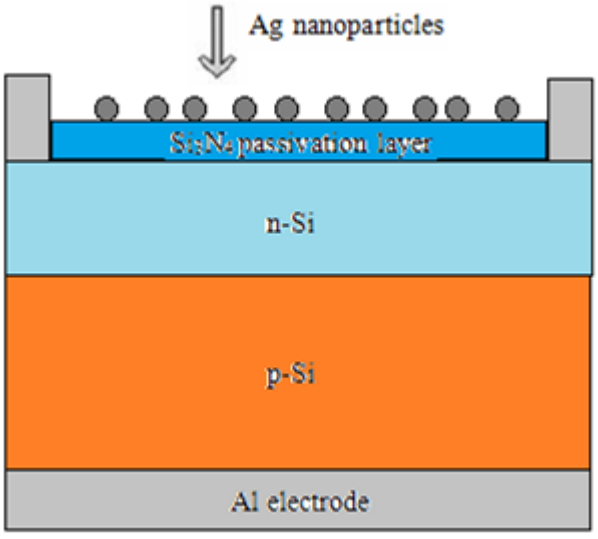

Figure 3-5. Monocrystalline Si solar cells with silver nanoparticles

Anti-reflection films are made of silver nanoparticles attached to the substrate. Let the transmittance be T_0, total area-S, total cross-sectional area-S_{Ag}, intensity of the incident light-I. Then we have the following relationships:

The light flux passes through the area with particles: $W_{Ag} = Q_{sca} S_{Ag} I$, (11)

The light flux passes through the area without particles: $W_0 = T_0 (SI - Q_{ext} S_{Ag} I)$, (12)

Total flux： $W = W_{Ag} + W_0$, (13)

Transmittance of the film: $T = \frac{W}{IS}$, (14)

Let the surface density of the particles be σ , then $S_{Ag} = \sigma S \cdot \pi R^2 = kS$, (15)

Applying (11), (12), (13), (14) in (15),

$$T = (Q_{sca} - T_0 Q_{ext})k + T_0 \text{ , (16)}$$

With a fixed radius, we are interested in finding the optimal k (or best σ) to make the transmittance T maximum. Apply (15) in (12),

$$W_0 = T_0 SI(1 - Q_{ext} k) \text{ , } 1 - Q_{ext} k \geq 0 \Rightarrow k \leq \frac{1}{Q_{ext}} \text{ , (17)}$$

(i) For $k > \frac{1}{Q_{ext}}$, (17) fails because the adjacent particles is to close and the energy received by per particle is so small that the LSP cannot be induced adequately. This is unfavorable and T decreases with the increasing of k. T eventually tends to be 0.02 with a very large k. Actually, the film becomes a silver mirror.

(ii) For $0 \le k \le \frac{1}{Q_{ext}}$, (16) shows that T has a positive correlation with k. When $k = \frac{1}{Q_{ext}}$, T reaches the maximum value $T = \frac{Q_{sca}}{Q_{ext}}$.

We found the optimal surface density, $\sigma(\lambda) = \frac{1}{\pi R^2 Q_{ext}(\lambda)}$ where Qext is a function of wavelength. The power density of the sunshine is maximum at the wavelength of about 500nm. So $\hat{\sigma} = \frac{1}{\pi R^2 Q_{ext}(500nm)}$ can be taken as the optimal surface density for the sunlight. Then we get the $R - \hat{\sigma}$ curves as shown in Fig. 3-6.

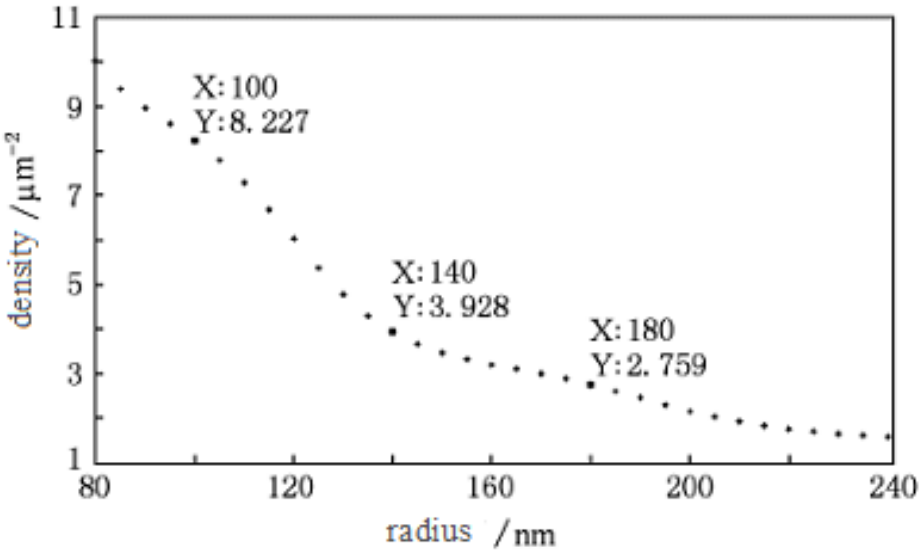

Figure 3-6. Optimal surface particle density vs radius of the Ag nanoparticles

Enhancement of the light current, $PE(\lambda) = \frac{T(\lambda) - T_0(\lambda)}{T_0(\lambda)}$, (18)

We calculated the $PE(\lambda)$ curves for the Si3N4 substrate deposited with the Ag nanoparticles with the radius of 20, 40, 60, 80, 100, 140 and 180nm as shown in Fig. 3-7.(Each of them reaches the optimal surface density).

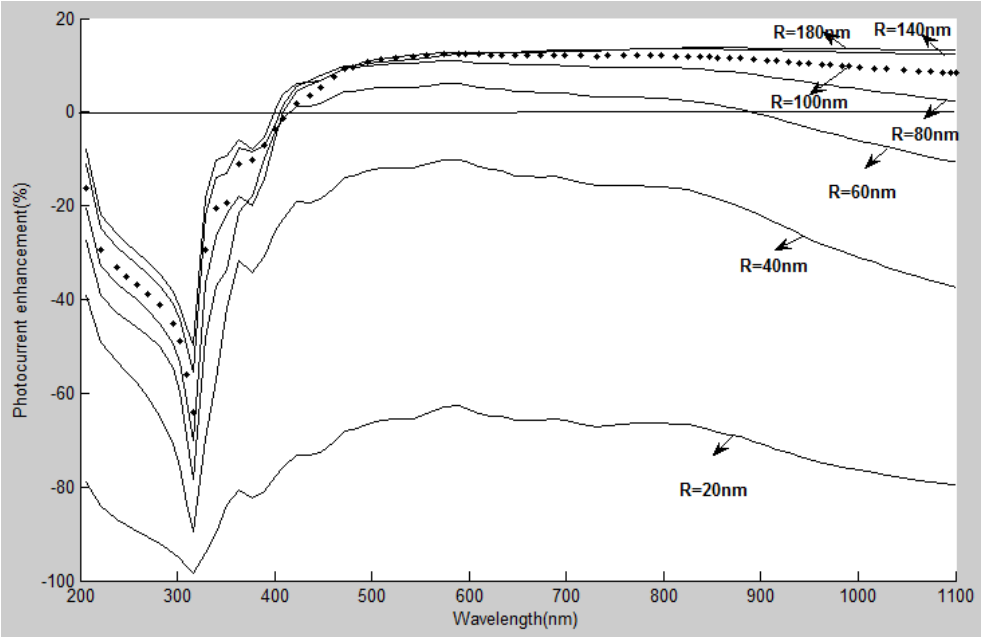

Fig. 3-7 Photocurrent enhancement of the antireflection films using Ag nanoparticles with different radius

From Fig.4 , the photocurrent enhancement becomes larger with the increasing radius. PE is positive for 400-1100nm wavelength when the radius is beyond 80nm; PE changes fairly minor when the radius is above 140nm. So the radius of the particles used in the antireflection films should be larger than 80nm. (The surface density should also set to be the optimal value).

A research group of UK[21] annealed the silver nanoparticles and got them with a generally uniform radius. They deposited the particles onto the substrate onto the silicon solar cell. They found that the forward scattering was strong when the radius reached 100nm and the transmittance was enhanced. This just proved our discussion and results.

We take the c-Si solar cells from industrial production for example. The efficiency of the solar cells is in the range of 15-19%. Ag nanoparticles with the radius of 180nm were deposited on top of the solar cells and the density was controlled to be $2.759\ \mu m^{-2}$ (optimal).

From the solar spectrum of standard AM1.5 given by ASTMG137[24,] we got the average photocurrent enhancement,

$$\overline{PE} = \frac{\int_{380nm}^{1100nm} PE(\lambda)S(\lambda)d\lambda}{\int_{380nm}^{1100nm} S(\lambda)d\lambda} \quad , (19)$$

where $S(\lambda)$ is the spectral intensity. Using (19), we obtained the average photocurrent enhancement which is equal to 13.37%.

We simulated a sample of c-Si solar cell before and after depositing Ag nanoparticles and got the volt-ampere characteristic curves (Fig. 3-8).

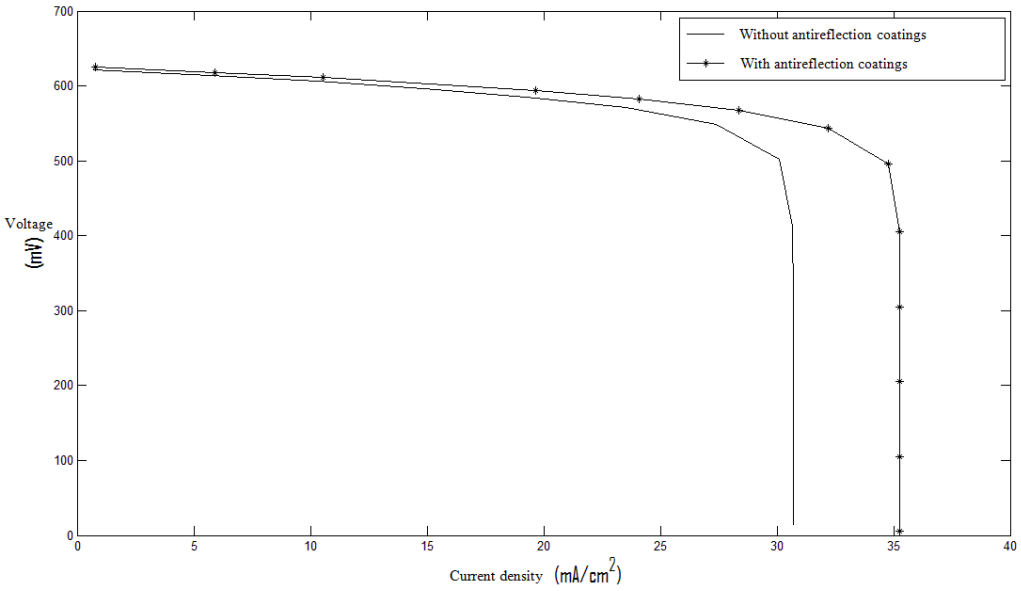

Figure 3-8. Volt-ampere characteristics of c-Si solar cells

The main characteristic parameters were obtained (Tab. 3-1). It can be observed from the solar cell with antireflection coatings that the short circuit current density Jsc is obviously improved. The open voltage is slightly increased. And the variation for the filling factor FF is very small. Generally, the conversion efficiency is increased from 15.39% to 17.59%. The enhancement is noticeable.

Table 3-1. The variation of the parameters of the solar cells with and without the anti-reflection coatings

Samples	Jsc(mA/cm2)	Voc(mv)	FF(%)	η（%）
Without coatings	30.71	622.9	80.45	15.39
With coatings	35.28	626.5	79.58	17.59

3.3.3 HIT SOLAR CELLS WITH PLASMONIC BUFFER LAYERS

We perform numerical calculations to the HIT solar cells with the plasmonic i layer, and find the proper parameters to improve the efficiency.

So far, the simulation of solar cells is usually solving the Poisson equations and there are many different ways to do this work. For example, the Scharfetter-Gummel method solves the Poisson equations and simulates solar cells[22].

The Scharfetter-Gummel method provides an optimal way to deal with the drift diffusion equations for carrier transportations. For one dimensional transportation problem in the spatial variable x, let n(x, t) be the density of the carriers (electrons or holes). Then the key expression is the continuity equation and the drift diffusion equation[23]:

$$\frac{\partial \mathrm{n}}{\partial t} = -\frac{\partial \mathrm{j}}{\partial x}, \qquad (20)$$

$$j = -D\frac{\partial \mathrm{n}}{\partial x} + v(x,t)n, \qquad (21)$$

where j is the carrier current density, D is the diffusivity, and v(x,t) is the drift velocity. With a uniform mesh, the discrete form of the continuity equation is expressed as:

$$\frac{\partial \mathrm{n_i}}{\partial t} = -\frac{j_{i+1/2} - j_{i-1/2}}{\Delta} = \frac{j_{i-1/2} - j_{i+1/2}}{\Delta}. \qquad (22)$$

Then the Scharfetter-Gummel method is to find the optimum approximation solutions for this equation.

The appearance of software call AFORS-HET highly simplify the calculations for simulating solar cells and also improved the precision. AFORS-HET was developed by the Hahn-Meitner Institute of Germany. It focuses on the simulation of heterojunction solar cells. With the software, we can simulate many different structures, factors and their influence to the solar cells. With the transient mode, the AFO, we can also observe the physical processes, store and change the data, make analysis and comparisons. The user interface is shown in Figure 3-9[24].

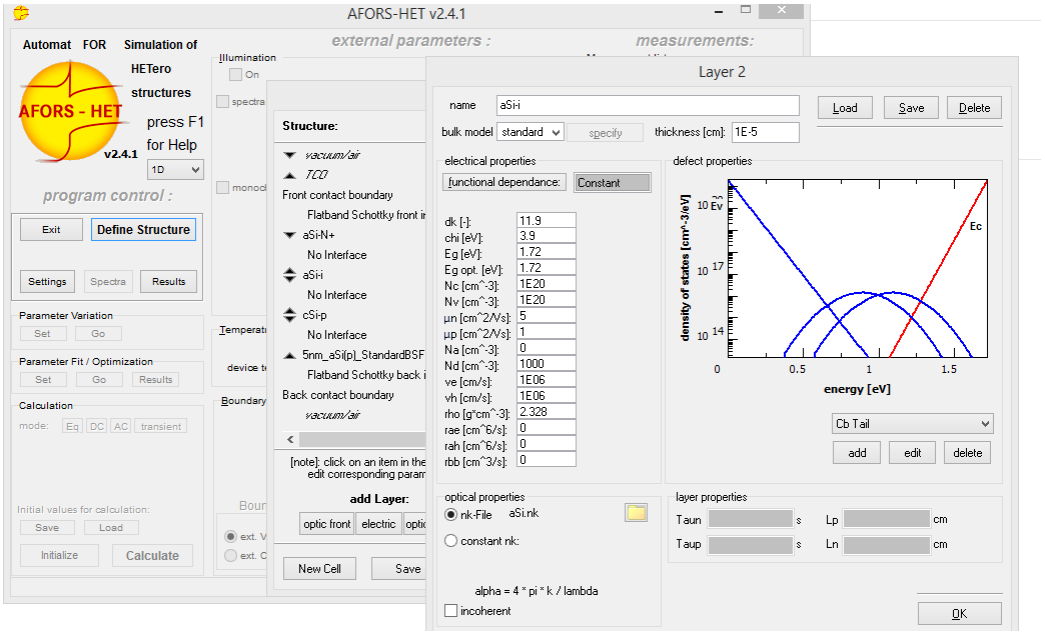

Figure 3-9 The interface of AFORS HET

Figure 3-10 shows the structure of the HIT solar cells with the plasmonic i layer. The substrate is p type c-Si with the thickness of 300µm. The ITO(80nm), Al back surface field, emitter junction (n+) and c-Si (p) have a parallel structure. The reflectivity is 0.1 for the front surface and 1 for the back surface. The light source is the standard AM1.5 spectrum of the sun[25]. The energy flow density is 100mW/cm^2.

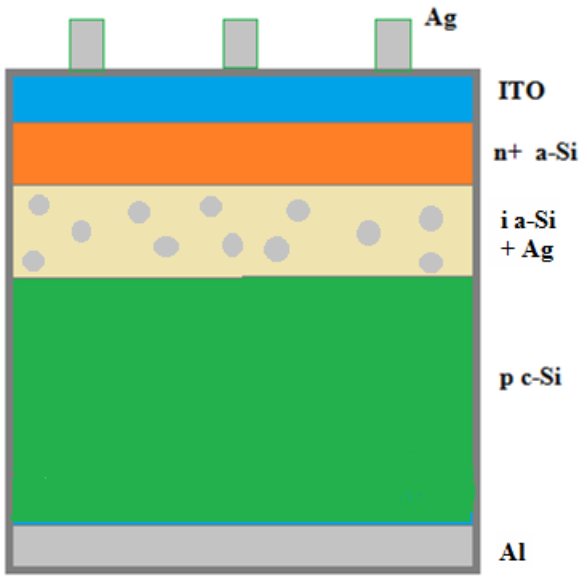

Figure 3-10 The structure of the HIT solar cell with plasmonic i layer

In the i layer, the radius of Ag nanoparticles is 100nm and the filling factor is 0.1.

The defect model of the emitter (a-Si) is DOS (density of states), which mainly consists two forms. 1).The states of the first form include two parts. One part in the top half of the band gap as the acceptor-like states, and another part lies in the bottom half as the donor like states.These band-tail states have an exponential distribution. 2) The states of the second form is in the middle of the band gap. They are induced by the dangling bonds and have a double Gaussian distribution. The parameters are shown in Table 3-2.

Table 3-2 The simulation parameters of the HIT solar cells

	Thickness(cm)	Electron affinity(eV)	Band gap(eV)	DOS of conduction band(cm^{-3})	DOS of valance band(cm^{-3})	Electron mobility (cm2V-1s-1)	Hole mobility (cm2V-1s-1)	Doping concentration of donor(cm-3)	Doping concentration of acceptor(cm^{-3})
a-Si (n+)	3×10^{-6}	3.9	1.72	1020	1020	5	1	1020	0
a-Si (i)	2.2×10^{-5}~2.8×10^{-5}	3.9	1.72	1020	1020	5	1	0	0
c-Si(p)	0.03	4.05	1.124	2.8×10^{19}	1.04×10^{19}	1041	412.9	0	1.5×10^{16}

An important parameter for solar cell is EQE(external quantum efficiency) , usually referred to as the incident photon-to-current conversion efficiency. EQE is a function of the wavelength and is dependent on LHE (light harvesting efficiency). We calculated the LHE of the HIT solar cells with/without the plasmonic layer (Fig. 3-11).

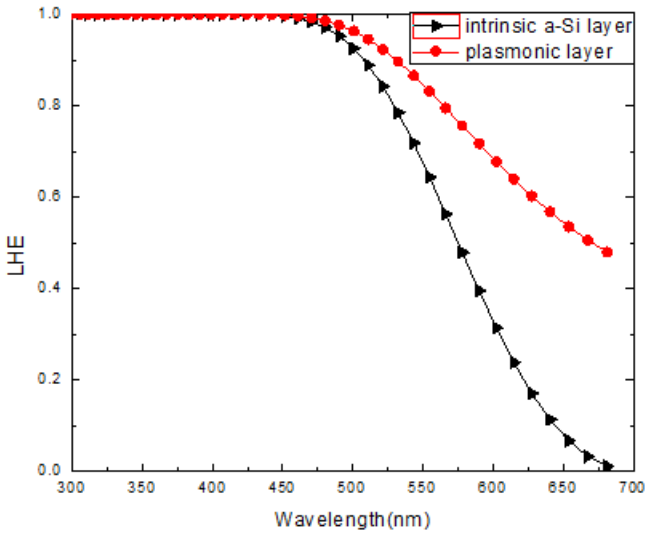

Figure 3-11 The light harvesting efficiency of HIT solar cells

The i layer here is set to be 220nm. The figure clearly shows that there is an effective enhancement in the wavelength from 500nm to 700nm.

The energy conversion efficiency for the HIT solar cells is calculated (Figure 3-12). The thickness of the i layer ranges from 220nm to 280nm. Without plasmonic layers, The efficiency is on the scale of 18.2%~19.0%. For the solar cells with plasmonic i layer, the efficiency is highly increased up to over 28.3%. Thus, there is a great improvement for the performance of the HIT solar cells.

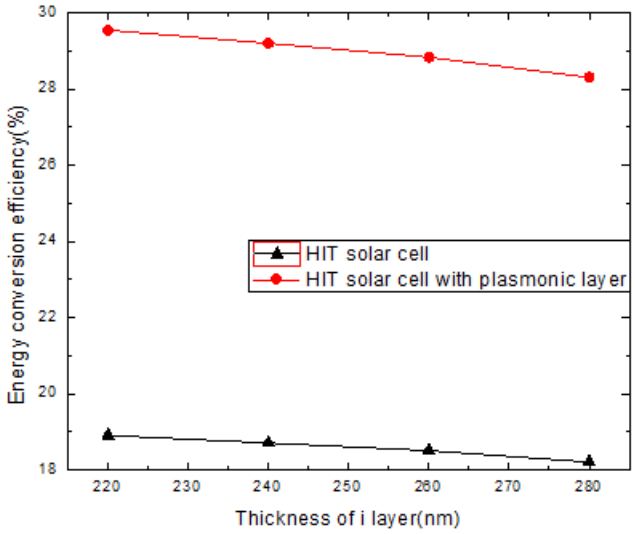

Figure 3-12. The energy conversion efficiency of HIT solar cells

4. BAND GAP AND CONDUCTANCE TALORING OF SEMICONDUCTORS (PREVIOUS WORK INCLUDED)

4.1 BACKGROUND

Band gap theory is a approximation to study the optical and electrical properties of semiconductors. Solid state materials are made of atoms and each atom has a core and some outer shell electrons. All of them are in constant motion. In order to reduce the problem, the atomic cores are assumed to be fixed and arranged periodically. And each electron moves in the periodic field of the atom core(also involved in the mean field cause by other electrons). F. Bloch first introduced this theory and it has been the fundamentals of solid state physics and semiconductor science. Semiconductors are classified by the fully occupied valence band and unoccupied conduction band. With the small band gap between these two bands, it takes a certain amount of energy to excite the electrons from the valence to conduction band[26]. Valence band means that the band of energy where all of the valence electrons reside and are involved in the highest energy molecular orbital. And conduction band is the range of electron energies enough to free an electron from binding with its atom to move freely within the lattice of the material as a delocalized electron.

Band gap engineering is to create artificial modified semiconductor materials in which the structure and value of the band gap can be tailored and optimized electrical properties can be obtained.

For solar cells, the band gap of each layer is extremely significant because it influences many parameters such as the absorptance of the solar spectrum and the open circuit voltage. With the development of band gap engineering, changing the band gap of Si has been very simple and tandem solar cells have been introduced with this technology. Tandem solar cells have many layers with different band gap. The incident photons reached the layer with a larger band gap at first and gradually goes in to the layer with a smaller band gap. This is a good match with the photon energy and the spectrum absorptance is very high. Thus, the tandem solar cell can achieve a high efficiency, usually over 35%.

However, tailoring the band gap of some functional thin films of solar cells is quite hard. For example, the transparent conductive oxide(TCO) is the top electrode of thin film solar cells. It requires the properties of high transmittance and low resistance at the same time. High transmittance of photons means the band gap should be wide enough but a simple widening treatment by doping elements usually leads to a low density of carriers. Then the carrier mobility must be tuned to be big enough because the resistivity is required to be very low. So optimizing the TCO is a complicate work. We will study the properties of ZnO based TCO and provide solutions to tailor the band gap and resistivity.

ZnO crystallizes in a stable wurtzite structure in nature. Its compounds such as ZnO:Al and ZnO:Mg have widely used in solar cells, phosphors and varistors. Intensive studies have shown that ZnO:IIIA films are good TCO because its high transmittance and low resistivity. Kim et al. discovered that there is a large optical band gap variation in

ZnO:In[27]. The band gap renormalization effect in ZnO:Ga was observed by Ye et al.[28] . Despite these studies, co-doping studies is still few and in this work we use both IIA and IIIA co-doping into ZnO thin films and investigate the physical properties.[29]

4.2 EFEECTS OF IIA doping ON ZnO

From first principle calculations and density functional theory[30-33], we compute the band gap, density of states(DOS), and lattice constant of ZnO:Mg. Norm- conserving pseudo potentials are used to describe the interactions between ionic cores and valence electrons. The wave function is expanded into plane wave energy functions and the cutoff energy is 380 eV. The simulation is iterated to self consistency with a grid of $6\times6\times6$ k-points in the reciprocal space.

For Mg contents of 0, 8.33, 12.50, 16.67, 25.00, 33.33, 50.00, and 58.33 percent, the lattice constant of ZnO:Mg is obtained. (Tab. 4-1)

Table 4-1. Calculated lattice parameters a and c of ZnO:Mg

Mg content (at. %)	0	8.33	12.5	16.67	25	33.33	50	58.33
Lattice constant *a* (Å)	3.2497	3.2463	3.2426	3.2491	3.2488	3.2489	3.2497	3.2470
Lattice constant *c* (Å)	5.1868	5.1667	5.1618	5.1604	5.1523	5.1403	5.1050	5.1138

Compared with the calculated intrinsic results (a=3.2479 Å, c=5.1868 Å) and the standard value of ZnO (a=3.2500 Å, c=5.2040 Å), the difference is less than 0.5%. Thus, the calculation has a high precision. With the increase of Mg content, the parameter c

decreases and a almost does not change except for an initial decrease, consistent with the experimental results[34, 35].

The band gap of ZnO:Mg is shown in figure 4-1. The band gap has a approximately linear relation against the Mg content, and the calculation results are in good agreement with the experimental values.[34]

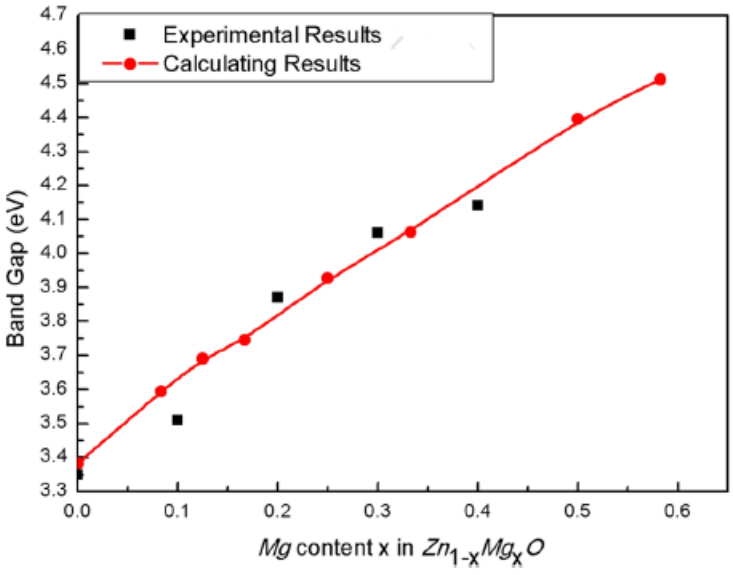

Figure 4-1. Band gap of ZnO:Mg against Mg content

From band gap theory and quantum chemistry, the position of the conducting band of ZnO is determined by Zn-4s state[29]. The Mg doping makes the electronic cloud of O approach Mg and move away from Zn, resulting in an increase of the bond length of Zn-O and the Zn-4s state is moving to a higher energy level. Then the Mg doping lead to the band gap widening of ZnO.

4.3 EFFECTS OF IIIA DOPING ON ZnO

We study the effects of IIIA doping and find it plays a key role to tune the electronic properties of ZnO. The carrier mobility μ comes from multiple different scattering mechanisms and it satisfies Equa. 23[29].

$$\frac{1}{\mu}=\frac{1}{\mu_{\mathrm{i}}}+\frac{1}{\mu_g}+\frac{1}{\mu_l}. \qquad (23)$$

where μ_i, μ_g, and μ_l represent the mobilities from ionized impurity scattering, gain boundary scattering, and lattice vibration scattering. And they satisfy Equa. 24-26[29].

$$\mu_{\mathrm{i}}=\begin{cases}\kappa m_e^{-2/3}. & \deg enerate\\ (2/m_c^*)^{1/2}[\ln(1+\frac{\varepsilon E_F}{n_e^{1/3}Ze^2})]^{-1}\frac{\varepsilon^{1/2}E_F^{3/2}}{\pi e^3 n_e Z^2}. & non\ \deg enerate\end{cases}. \qquad (24)$$

$$\mu_{\mathrm{g}}=\mu_0 T^{-1/2}\exp(-\Delta E/k_B T). \qquad (25)$$

$$\mu_{\mathrm{l}}=(\frac{\pi}{3})^{1/3}\frac{eh^3 C_l}{(m_c^*)^2 E_d^2 k_B T n_e^{1/3}}\propto\frac{1}{T}. \qquad (26)$$

where e, h and n_e represent electron mass, Plank constant and electron concentration. Z is ion valence. ΔE and T denote the potential barrier of grain-boundary and the temperature. C_l and E_d are the elasticity modulus and the deformation potential constant.

From what we discussed above, ionized impurity scattering is the dominant factor for the carrier mobility of ZnO:IIIA in room temperature and can be calculated. As is shown in Fig 4-2, the carrier mobility μ tend to be proportional to $n_e^{-2/3}$ which has also been confirmed by experimental values. As $\sigma = n_e \mu e$, the conductivity will approximately be

proportional to $n_e^{1/3}$. All these discoveries indicate that electron concentration is very effective to reduce resistivity. A large number of experiments have shown that the electron concentration reaches maximum when Al content is 4at.%. The reason is that Al_2O_3 will inevitably appear to reduce the electron concentration when Al content exceeds 4at.% no matter which growing method is used. It is worth noting that the conductivity reaches maximum as well when Al content is 4at.%[36]. This is just consistent with our ratiocinations.

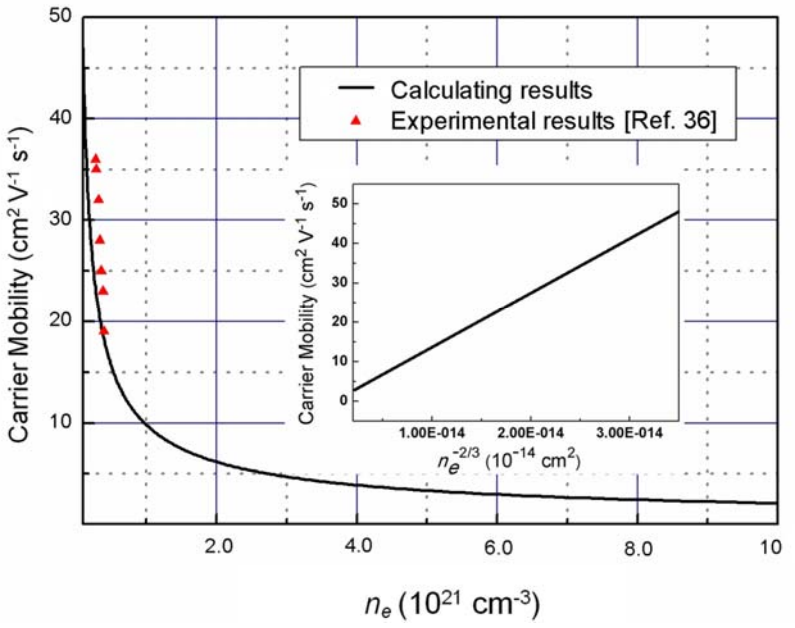

Figure 4-2. Carrier mobility of *ZnO:Al* as a function of the electron concentration. Inset: calculated carrier mobility as a function of $n_e^{-2/3}$.

From first principle calculations, we obtained the band gap of ZnO:Al. For Al doping, there is a band gap shift from Burstein-Moss effect[37], the band gap renormalization

effect[38], and the semiconductor-metal transition effect[39]. Fig. 4-3 shows the results considering one of the effects or all of them. When we take all the three effects into account, the result is in very good agreement with the experimental value[40]. The band gap can be expressed as a function of the electron concentration.

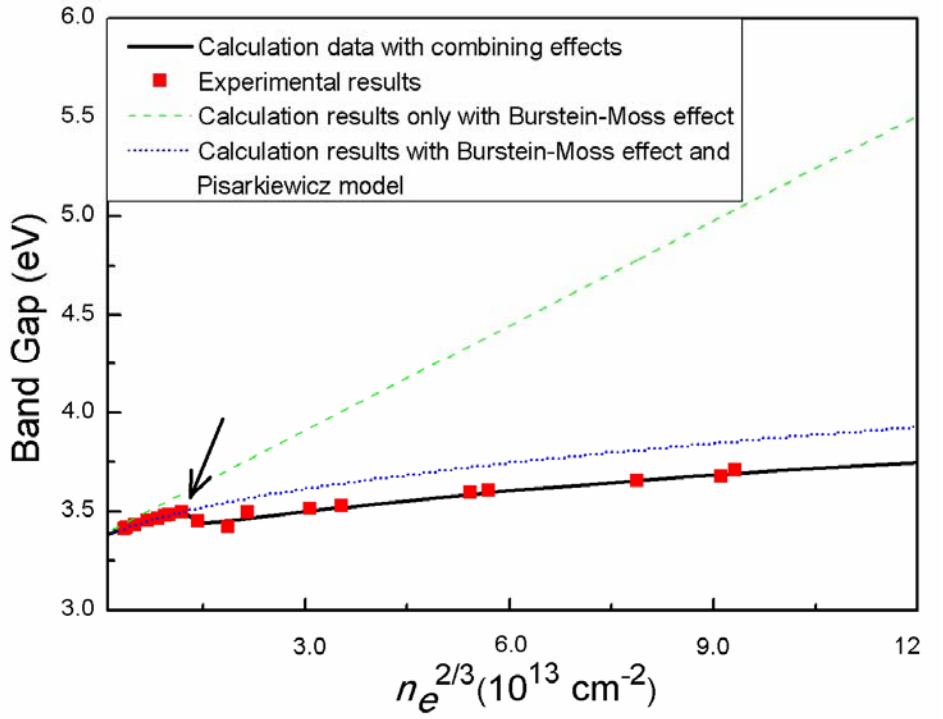

Figure 4-3. Band gap of ZnO:Al as a function of the electron concentration.

Electronic properties of ZnO doped with other IIIA element could also be studied using similar methods according to Mendeleev Law.

4.4 ZnO CO-DOPED WITH IIA AND IIIA

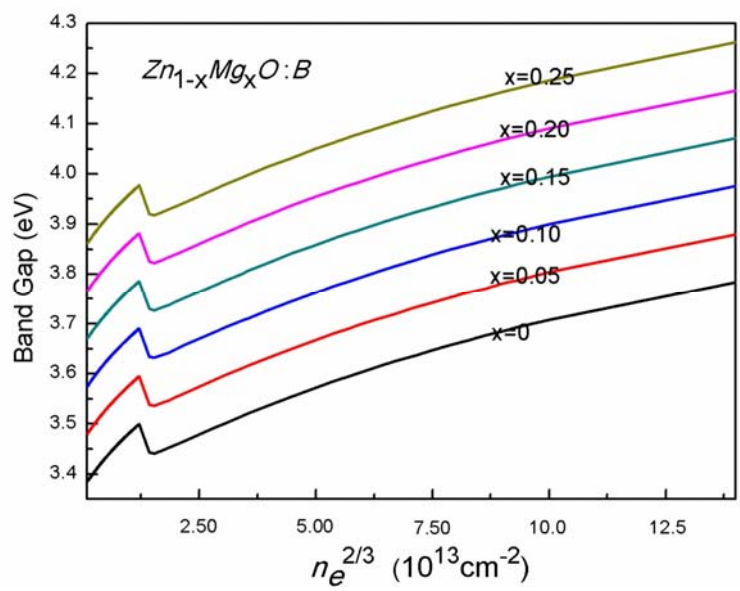

Figure 4-4. Calculated band gap of Zn1-xMgxO:B as a function of the electron concentration for x = 0, 0.05, 0.10, 0.15, 0.20.

Theoretically, with first principle calculations, and the effects we studied above, ZnO co-doped with IIA and IIIA can be calculated. For example, we calculated the band gap of ZnO:[Mg, B]. (Fig. 4-4).

Experimentally, ZnO films co-doped with Mg and B, called ZnO:[Mg,B] films, have been grown on the quartz substrates by metalorganic chemical vapor deposition (MOCVD)[29]. Source materials including gaseous H_2O, diethyl-zinc, methylcyclopenta-dienyl-magnesium, and borane (B_2H_6) have been carried into the MOCVD reaction chamber with high purity Ar gas. The following growth conditions have been used: substrate temperature 254 ^oC, diethyl-zinc temperature 20 ^oC, methylcyclopenta-dienyl-magnesium temperature 74 ^oC, H2O temperature 40 ^oC, H2O flow rate 50 sccm, diethyl-

zinc flow rate 10 sccm, total pressure 1.5 torr, and growth time 1h. The B2H6 flow rate has been varied between 0 and 5 sccm. In fact, we have firstly prepared Zn1-xMgxO (x=0.11) films whose the band gap is 3.576 eV, and then fabricated co-doped ZnO:[Mg,B] films of different B contents by controlling the B2H6 flow rate. Note that Zn1-xMgxO films of other band gaps between 3.37 and 5 eV can be readily obtained by varying the Mg contents.

We have measured the band gap, electron concentration, Hall mobility, and resistivity for the co-doped samples, as displayed in Fig. 4-5. As shown in the inset of Fig. 4-5(a), the band gap sharply increases with increasing B_2H_6 flow rate to 2.0 sccm, as expected, whereas it slightly decreases when the flow rate is over 2.0 sccm. The origin of this small decrease of the band gap is not clear at present and needs to be further investigated. Also, the carrier mobility clearly decreases with an increase of the carrier concentration since the more flow rate implies the more concentration, suggesting that the ionized impurity scattering is the dominant factor for the carrier mobility in the co-doped samples. In addition, the resistivity was detected to be reduced from 10^4 Ωcm (before B-doping) to 10^{-5} Ωcm. Apparently from the figure, the band gap and conductivity of ZnO films can be widely tuned by co-doping IIA and IIIA elements.

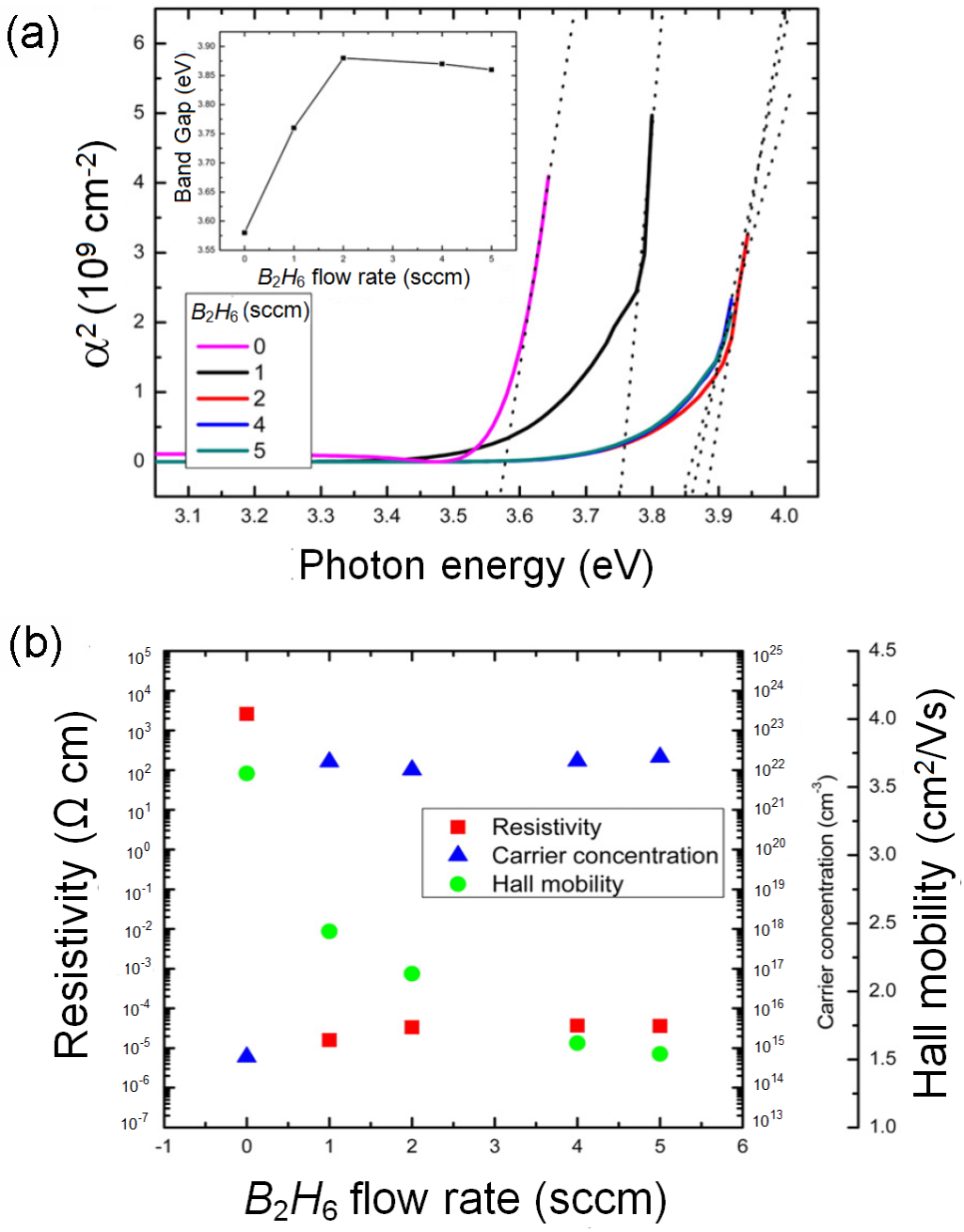

Figure 4-5. (a) Photon energy-dependent absorption coefficient α of *ZnO:*[*Mg*,*B*] films for various B_2H_6 flow rate. Inset: optical band gap of *ZnO:*[*Mg*,*B*] as a function of the B_2H_6 flow rate. (b) Electron concentration, Hall mobility, and conductivity of *ZnO:*[*Mg*,*B*] as a function of the B_2H_6 flow rate.

5. SUMMARY

This article introduced the principles, types and bottleneck of the development of solar cells. Advanced materials and nanotechnology have shown great significance in the field of photovoltaics. The properties and applications of ZnO based semiconductors and Ag based meta-materials are investigated. The light trapping properties of Ag nano-material is studied theoretically. The best particle radius and density is found for monocrystalline Si solar cell. The great improvement for HIT solar cells has been observed. For ZnO based semiconductors co-doped with IIA and IIIA elements, the optical and electronic properties are studied theoretically and experimentally, and the physical explanations are provided.

To sum up, this article obtained the following results:

a. Studied the optical properties of silver nanoparticles.

b. Simulated the monocrystalline Si solar cell with Ag nanoparticles. Obtained the characteristics of light current. Improved the energy conversion from 15.4% to 17.6%.

c. Modeled the HIT solar cells with plasmonic layer and enhanced the performance.

d. Studied the band gap and resistivity of ZnO thin films co-doped with IIA and IIIA.

e. Provide a powerful method to tailor the band gap and resistivity of ZnO based thin films at the same time.

The future work will focus on:

a. Analyze materials and processes cost.

b. Apply these techniques to other types of solar cells.

BIBLIOGRAPHY

[1] U.S. Energy Information Administration.

[2] Climate Change 2007: Synthesis Report.

[3] http://www.narucmeetings.org.

[4] Green, M. A., Emery, K., Hishikawa, Y., Warta, W. and Dunlop, E. D. (2014), Solar cell efficiency tables (version 43). Prog. Photovolt: Res. Appl., 22: 1–9.

[5] Green, M. A. (2003), "Crystalline and thin-film silicon solar cells: state of the art and future potential", Solar Energy 74 (3): 181–192.

[6] Scharber, Markus C., et al. "Design rules for donors in bulk‐heterojunction solar cells—Towards 10% energy‐conversion efficiency." Advanced Materials 18.6 (2006): 789-794.

[7] Kessler, Friedrich, and Dominik Rudmann. "Technological aspects of flexible CIGS solar cells and modules." Solar Energy 77.6 (2004): 685-695.

[8] Noufi, Rommel, and Kenneth Zweibel. "High-efficiency CdTe and CIGS thin-film solar cells: highlights and challenges." Photovoltaic Energy Conversion, Conference Record of the 2006 IEEE 4th World Conference on. Vol. 1. IEEE, 2006.

[9] Hecht (2003), p. 120, eq.(4.57)

[10] Eduardo Lorenzo (1994). Solar Electricity: Engineering of Photovoltaic Systems. Progensa.ISBN 84-86505-55-0.

[11] K. Taretto, U. Rau, J. H. Werner, Appl. Phys. A, 77, 865-871 (2003) and K. Taretto, U. Rau, J. H. Werner, Appl. Phys. A, 86, 151 (2007)

[12] Tsunomura, Yasufumi, et al. "Twenty-two percent efficiency HIT solar cell."Solar Energy Materials and Solar Cells 93.6 (2009): 670-673.

[13] Willets, Katherine A., and Richard P. Van Duyne. "Localized surface plasmon resonance spectroscopy and sensing." Annu. Rev. Phys. Chem. 58 (2007): 267-297.

[14] P. B. Johnson and R. W. Christy. Optical Constants of the Noble Metals, Phys. Rev. B 6, 4370-4379 (1972)

[15] Ordal, M. A., et al. "Optical properties of the metals al, co, cu, au, fe, pb, ni, pd, pt, ag, ti, and w in the infrared and far infrared." Applied Optics 22.7 (1983): 1099-1119.

[16] Bohren, Craig F., and Donald R. Huffman. Absorption and scattering of light by small particles. John Wiley & Sons, 2008.

[17] "The beer-lambert law." Journal of chemical education 39, no. 7 (1962): 333.
[18] Kravets, V. G., et al. "Plasmonic blackbody: Strong absorption of light by metal nanoparticles embedded in a dielectric matrix." Physical Review B 81.16 (2010): 165401.
[19] Reference Solar Spectral Irradiance: Air Mass 1.5NREL retrieved 1 May 2011
[20] Dhatt, Gouri, Emmanuel Lefrançois, and Gilbert Touzot. Finite element method. John Wiley & Sons, 2012.
[21] Temple T L, Mahanama G D K, Reehal H S, Bagnall D M 2009 Solar Energy Materials & Solar Cells 93 1978.
[22] Scharfetter, D. L., and H_K Gummel. "Large-signal analysis of a silicon read diode oscillator." Electron Devices, IEEE Transactions on 16.1 (1969): 64-77.
[23] Kulikovsky, A. A. "A more accurate Scharfetter-Gummel algorithm of electron transport for semiconductor and gas discharge simulation." Journal of computational physics 119.1 (1995): 149-155.
[24] Froitzheim, A., et al. "AFORS-HET: a computer-program for the simulation of heterojunction solar cells to be distributed for public use." Photovoltaic Energy Conversion, 2003. Proceedings of 3rd World Conference on. Vol. 1. IEEE, 2003.
[25] http://rredc.nrel.gov/solar/spectra/am1.5/ASTMG173/ASTMG173.html.
[26] Neamen, Donald (2006). An Introduction to Semiconductor Devices (1st ed.) McGraw-Hill.

[27] K. J. Kim and Y. R. Park, Appl. Phys. Lett. 78, 4 (2001).
[28] J. D. Ye, S. L. Gu, S. M. Zhu, S. M. Liu, Y. D Zheng, R. Zhang, Y. Shi, Appl. Phys. Lett. 86, 19 (2005).
[29] Han, T., et al. "Band gap and electronic properties of wurtzite-structure ZnO co-doped with IIA and IIIA." Journal of Applied Physics 110.6 (2011): 063724.
[30] Ohno, Kaoru, Keivan Esfarjani, and Yoshiyuki Kawazoe. Ab Initio Methods. Springer Berlin Heidelberg, 1999.
[31] P. Hohenberg and W. Kohn, Phys. Rev. 136, B864 (1964).
[32] M. D. Segall, O. J. D. Lindan, M. J. Probert, C. J. Pickard, P.J. Hasnip, S. J. Clark, and M. C. Payne, J. Phys. Condens. Matter. 14, 2717 (2002).
[33] Y. Imai, M. Mukaida, and T. Tsunoda, Thin Solid Films. 381, 176 (2001).

[34] A. Kaushal and D. Kaur, Sol. Energy Mater. Sol. Cells 93, 193 (2009).

[35] F. K. Shan, B. I. Kim, G. X. Liu, Z. F. Liu, J. Y. Sohn, W. J. Lee, B. C. Shin, and Y. S. Yu, J. Appl. Phys. 95, 4772 (2004).

[36] J. G. Lu, Z. Z. Ye, Y. Z. Zeng, L. P. Zhu, L. Wang, J. Yuan, B. H. Zhao, Q. L. Liang, J. Appl. Phys. **100**, 073714, (2005).

[37] A. P. Roth, J. B. Webb, and D. F. Williams, Solid State Communications 39, 12, (1981).

[38] D. C. Reynolds, D. C. Look, and B, Jogai, J. Appl. Phys 88,5760 (2000).

[39] V. Bhosle, A. Tiwari, and J. Narayan, Appl. Phys. Lett. 88, 032106 (2006).

[40] J. G. Lu, S. Fujita, and Z. Z. Ye, J. Appl. Phys. **101**, 083705 (2007).